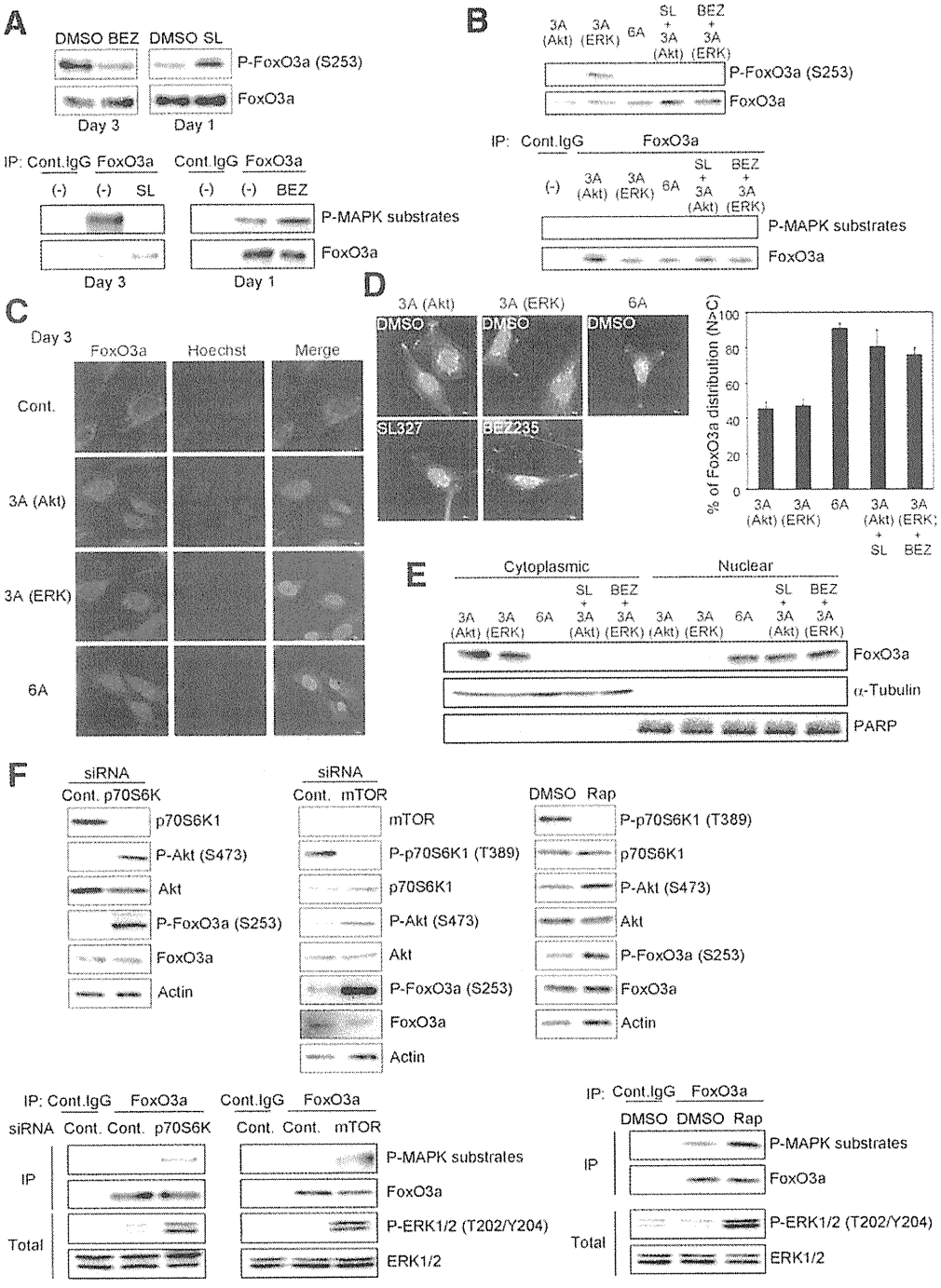

Figure 3. The PI3K/Akt/mammalian target of rapamycin (mTOR) and MEK/extracellular signal-regulated kinase (ERK) pathways, which are under cross-inhibitory regulation via mTOR-p70S6K, directly control FoxO3a phosphorylation at the Akt and ERK phosphorylation sites as well as its subcellular localization. SJ28P3 cancer stem-like cells (CSLCs) were cultured in the absence or presence of NVP-BEZ235 (BEZ, 1 μM) or SL327 (SL, 10 μM) for 3 days (**A**, left) or 1 day (**A**, right). The cells were then subjected to immunoblot analysis with the indicated antibodies (**A**, upper) or to immunoprecipitation (IP) with control IgG (Cont. IgG) or an anti-FoxO3a antibody, followed by immunoblot analysis with the indicated antibodies (**A**, lower). **(B–E):** SJ28P3 CSLCs were infected with an empty control vector or with lentiviral vectors expressing the 3A (Akt) (T32A/S253A/S315A), 3A (ERK) (S294A/S344A/S425A), or 6A (T32A/S253A/S315A, S294A/S344A/S425A) FoxO3a mutant. After 1-day, cells were treated with BEZ (1 μM) or SL (10 μM) for 3 days and subjected to immunoblot analysis with the indicated antibodies (**B**, upper), to IP with control IgG or an anti-FoxO3a antibody followed by immunoblot analysis with the indicated antibodies (**B**, lower) or to subcellular fractionation, with the amount of FoxO3a in the cytoplasmic and nuclear fractions being assessed by immunoblot analysis (**E**). Alternatively, cells were immunolabeled for FoxO3a (**C**, **D**, left). **(F):** SJ28P3 CSLCs were transfected with the indicated siRNAs or treated with rapamycin (50 nM). After 2 days, the cells were subjected to immunoblot analysis with the indicated antibodies (upper) or to IP with control IgG or an anti-FoxO3a antibody, followed by immunoblot analysis with the indicated antibodies (lower). Abbreviations: Cont., control; DMSO, dimethyl sulfoxide; ERK, extracellular signal-regulated kinase; mTOR, mammalian target of rapamycin; siRNA, short-interfering RNA; IP, immunoprecipitation; PARP, poly(ADP-ribose) polymerase; Rap, rapamycin.

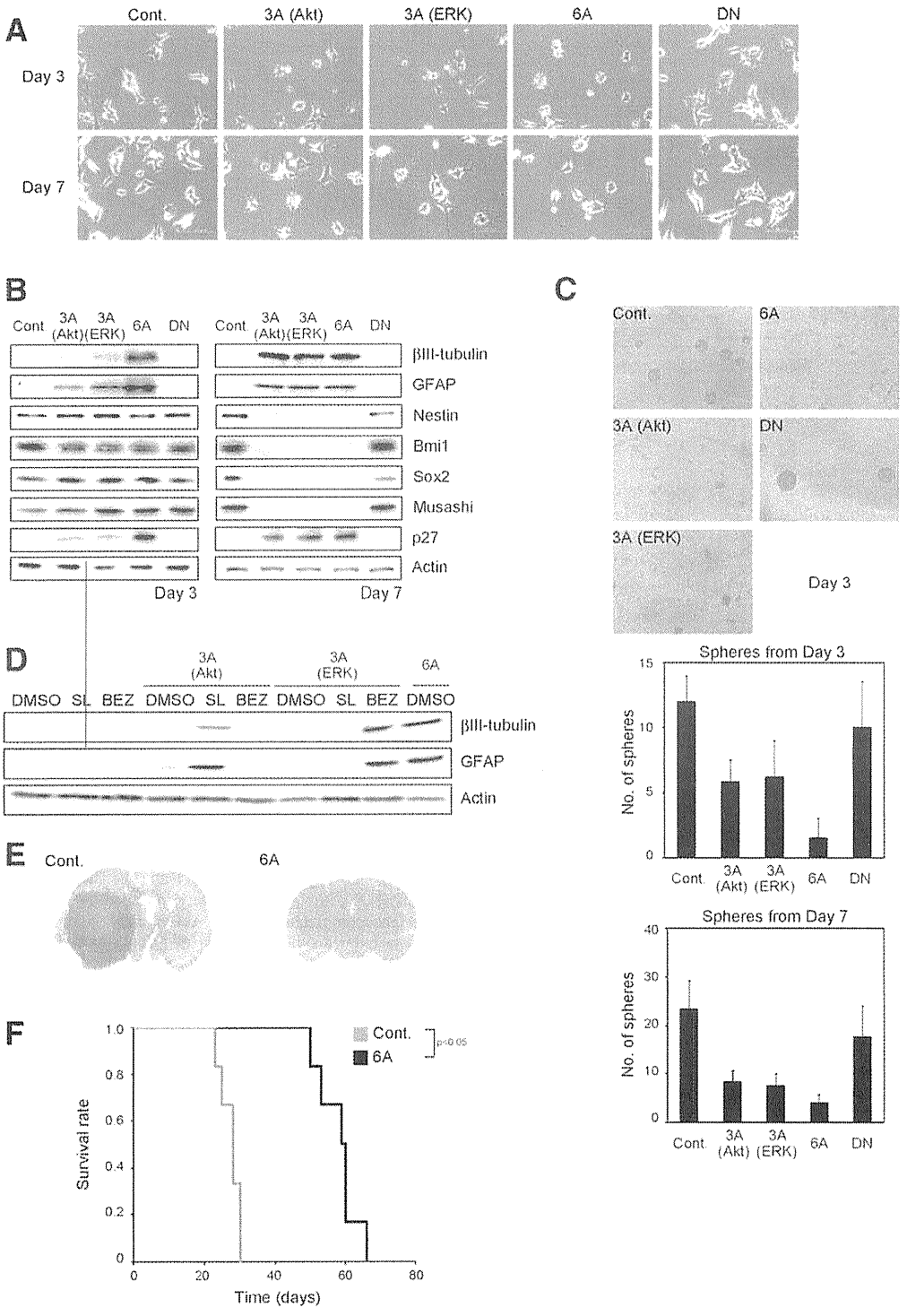

Figure 4. Expression of the Akt and extracellular signal-regulated kinase (ERK) phosphorylation site-defective FoxO3a mutant is sufficient to induce differentiation and inhibit tumorigenicity of glioblastoma cancer stem-like cells (CSLCs). SJ28P3 CSLCs were infected with an empty, control vector or with lentiviral vectors expressing the 3A (Akt) (T32A/S253A/S315A), 3A (ERK) (S294A/S344A/S425A), 6A (T32A/S253A/S315A, S294A/S344A/S425A), or a dominant-negative FoxO3a mutant. Approximately 3 or 7 days after infection, cells were observed under a phase-contrast microscope (**A**), subjected to immunoblot analysis with the indicated antibodies (**B**) or to sphere formation assays (**C**). Alternatively, cells were treated, 1-day after infection, with NVP-BEZ235 (BEZ, 1 μM) or SL327 (SL, 10 μM) for 3 days, and cell lysates were subjected to immunoblot analysis with the indicated antibodies (**D**). (**E, F**): SJ28P3 CSLCs were infected with a control lentiviral vector or with a lentiviral vector expressing the 6A FoxO3a mutant. Approximately 7 days after infection, the cells (1×10^4) were injected intracranially into BALB/c-nu/nu mice. The mice were sacrificed 30 days after intracranial injection, and brain tissue sections were stained with H&E (**E**). Survival of mice (six mice per group) was evaluated by Kaplan-Meier analysis (**F**). Abbreviations: Cont., control vector; DMSO, dimethyl sulfoxide; DN, dominant-negative; ERK, extracellular signal-regulated kinase; GFAP, glial fibrillary acidic protein.

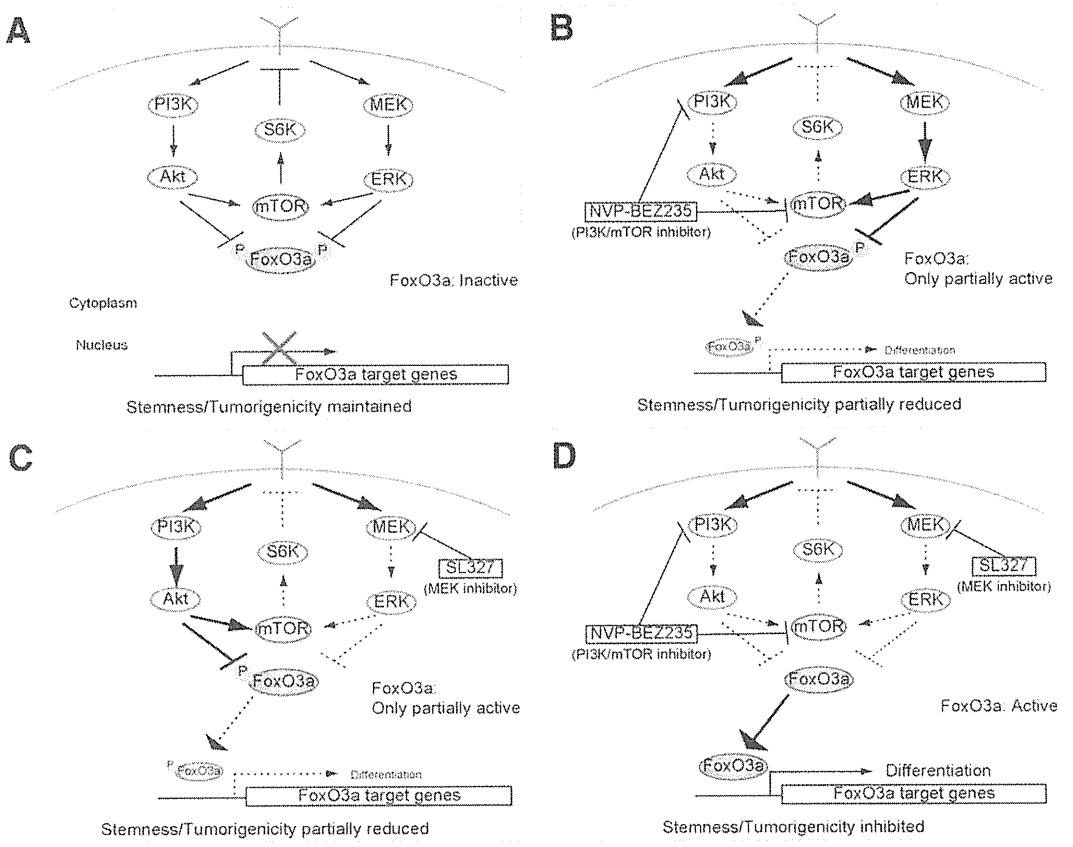

Figure 5. Schematic summary for FoxO3a-mediated control of glioblastoma cancer stem-like cell (CSLC) differentiation and tumorigenicity by the PI3K/Akt/mammalian target of rapamycin (mTOR) and MEK/extracellular signal-regulated kinase (ERK) pathways. **(A):** The PI3K/Akt/mTOR and MEK/ERK pathways, which negatively regulate themselves and each other via p70S6K (S6K), are active in glioblastoma CSLCs. FoxO3a phosphorylated by both Akt and ERK is efficiently retained in the cytoplasm and remains inactive. **(B):** When the PI3K/Akt/mTOR pathway is selectively inhibited, FoxO3a phosphorylated by ERK can still be retained in the cytoplasm. Loss of PI3K/Akt/mTOR pathway-mediated inhibition further activates the MEK/ERK pathway, which contributes to increased phosphorylation of FoxO3a at the ERK sites and consequently, to the maintenance of the stem cell state. **(C):** The same is true when the MEK/ERK pathway is selectively inhibited. **(D):** Upon concurrent inhibition of the PI3K/Akt/mTOR and MEK/ERK pathways, FoxO3a is no longer phosphorylated either by Akt or ERK. Nonphosphorylated FoxO3a efficiently translocates to the nucleus, where it activates its target genes associated with differentiation of glioblastoma CSLCs and suppresses their tumorigenicity. Abbreviations: ERK, extracellular signal-regulated kinase; MEK, mitogen-activated protein/extracellular signal-regulated kinase kinase; mTOR, mammalian target of rapamycin.

accumulates in the nucleus when it is phosphorylated neither by Akt nor ERK.

We have previously demonstrated that crosstalk between the PI3K/Akt and MEK/ERK pathways through an mTOR-p70S6K axis-dependent feedback loop is involved in the maintenance of self-renewal and tumorigenicity of glioblastoma CSLCs [14]. Therefore, we investigated the possibility that Akt and ERK phosphorylation of FoxO3a is under the control of this crosstalk in glioblastoma CSLCs. In support of this possibility, the MEK inhibitors SL327 and U0126 increased FoxO3a phosphorylation at Ser253, and the PI3K/mTOR inhibitor NVP-BEZ235 did so at ERK consensus sequences (Fig. 3A, right; Supporting Information Fig. 3A, right). Essentially identical results were obtained when MEK1/2 or PI3K isoforms and mTOR were knocked down (Supporting Information Fig. 5). As reported earlier [14], inactivation of the mTOR-p70S6K axis, by means of siRNA-mediated knockdown or a pharmacological inhibitor, induced the phosphorylation of upstream Akt and ERK. Under these conditions, FoxO3a phosphorylation at the Akt and ERK phosphorylation sites was apparently increased (Fig. 3F; Supporting Information Fig. 3B). Thus, the data suggest that, in glioblastoma CSLCs, FoxO3a is regulated through phosphorylation by Akt and ERK, both of which are under the control of the negative feedback loop involving the downstream mTOR-p70S6K axis.

Expression of FoxO3a Lacking Akt- and ERK-Mediated Phosphorylation is Sufficient to Induce Differentiation and to Inhibit Self-Renewal and Tumorigenicity of Glioblastoma CSLCs

We then questioned the impact of Akt- and/or ERK-mediated phosphorylation of FoxO3a on the maintenance of stem cell-like properties of glioblastoma CSLCs. To this end, we again took advantage of the FoxO3a mutants lacking Akt and/or ERK phosphorylation sites. On day 3, glioblastoma CSLCs transduced with the expression vector encoding the 6A mutant showed prominent morphological changes characterized by extension of cellular processes (Fig. 4A), suggesting that the cells may be undergoing differentiation. Cells expressing the 3A mutants at comparable levels to the 6A mutant (Supporting Information Fig. 4) showed essentially similar morphological changes but apparently in a much more modest manner (Fig. 4A). Immunoblot analysis revealed the parallel increase of differentiation markers, GFAP and βIII-tubulin, together

with p27 in cells expressing the 3A and 6A mutants, quite consistent with the morphological changes (Fig. 4B). In addition, the 3A (Akt) and 3A (ERK) mutants, which were by themselves less efficient inducers of differentiation than the 6A mutant, efficiently induced the expression of βIII-tubulin and GFAP in the presence of the MEK and PI3K/mTOR inhibitors, respectively (Fig. 4D). In contrast, increased expression of wild-type FoxO3a, which was not overexpressed as efficiently as the mutants probably due to increased protein degradation when compared with the nonphosphorylatable FoxO3a mutants [19], did not induce differentiation under the experimental condition (Supplementary Information Fig. 6). Thus, the results together suggest that the absence of Akt- and ERK-mediated phosphorylation cooperatively activates FoxO3a to induce differentiation of glioblastoma CSLCs. Although the differences between the 3A and 6A mutants became less prominent on day 7, this could be explained by the fact that these mutants are overexpressed and by saturation of the differentiation-inducing effect (Fig. 4A, 4B). Significantly, we found that the expression of neural stem/progenitor cell markers such as Nestin, Bmi1, Sox2, and Musashi remains unchanged on day 3 but is inhibited on day 7, which may imply that FoxO3a activation is sufficient to inhibit stem/progenitor cell marker expression but induces differentiation independently of their inhibition. We also examined the effect of FoxO3a mutant expression on the self-renewal capacity of glioblastoma CSLCs. In close correlation to their ability to inhibit the expression of stem/progenitor cell markers, the three FoxO3a mutants inhibited sphere formation by glioblastoma CSLCs (Fig. 4C). Similar results were obtained when glioblastoma CSLCs (#38) derived from another patient were used (Supporting Information Fig. 7).

Since the 6A FoxO3a mutant was so efficient at inducing differentiation as well as in depleting the pool of self-renewing glioblastoma CSLCs, we next asked whether the 6A mutant expression could also inhibit their tumorigenic potential. To test this idea, glioblastoma CSLCs transduced with the expression vector for the 6A mutant were injected intracranially into immunodeficient mice, and the animals were monitored for brain tumor formation and survival (Fig. 4E, 4F). Although all animals injected with cells transduced with the control vector died within one month after injection (median survival is 28 days), animals injected with cells transduced with the 6A mutant expression vector survived significantly longer (median survival is 59.5 days). In a parallel experiment, mice were sacrificed 30 days after injection, and the brains were examined for the presence of tumors. While massive tumor growth was confirmed in control animals, no visible tumor growth was detected in animals receiving glioblastoma CSLCs transduced with the 6A mutant expression vector. Collectively, the results suggest that forced activation of the FoxO3a pathway via 6A mutant expression by itself is sufficient to induce differentiation and reduce the tumorigenic potential of glioblastoma CSLCs without requiring inhibition of the PI3K/Akt/mTOR and MEK/ERK pathways.

Discussion

We have recently shown that the PI3K/Akt/mTOR and MEK/ERK pathways, which are aberrantly activated in glioblastomas, crosstalk via a p70S6K-mediated negative feedback mechanism and coordinately regulate differentiation, self-renewal, and tumorigenicity of glioblastoma CSLCs [14]. Here in this study, we have provided evidence that FoxO3a is at least one of the missing links connecting the two pathways. We have shown that concurrent inhibition of the PI3K/Akt/mTOR and MEK/ERK pathways, which negatively regulate each other in glioblastoma CSLCs, causes efficient loss of phosphorylation at Akt and ERK phosphorylation sites, nuclear accumulation, and increased transcriptional activity of FoxO3a, that FoxO3a is required for the differentiation of glioblastoma CSLCs induced by the inhibition of these signaling pathways, and that forced activation of the FoxO3a pathway, conversely, is sufficient to induce differentiation and inhibit self-renewal and tumorigenicity of glioblastoma CSLCs. These findings demonstrate that FoxO3a functions at the convergence of the PI3K/Akt/mTOR and MEK/ERK pathways controlling glioblastoma CSLCs (schematically summarized in Fig. 5). Intriguingly, we have also discovered in the course of this study that oxidative stress activates FoxO3a, induces differentiation, and inhibits self-renewal as well as the tumorigenicity of glioblastoma CSLCs at least in part in a FoxO3a-dependent manner yet without affecting the PI3K/mTOR and MEK/ERK pathways (Supporting Information Fig. 8). This additional observation further suggests the possibility that FoxO3a may function not only as a signal integrator specific to the PI3K/Akt/mTOR and MEK/ERK pathways but may also have a more general and pivotal role in the control of glioblastoma CSLCs.

To our knowledge, there are only a limited number of, and seemingly conflicting, reports on the role of FoxO3a in the control of stem cell-like properties of CSLCs. In prostate cancer, the FoxO3a pathway was more activated in the non-CSLC population than in the CSLC population, and FoxO3a knockdown led to expansion of the CSLC pool as well as to increased self-renewal and tumorigenic capacity [20]. In contrast, in chronic myeloid leukemia, leukemia-initiating cells (LICs) were enriched in cells exhibiting nuclear localization of FoxO3a, and FoxO3a deficiency impaired the leukemia-initiating potential of LICs [21]. Apparently, the contrasting roles of FoxO3a in the maintenance of CSLC properties documented in these reports suggest that FoxO3a may have different functions in CSLCs of different cancer types. In this regard, we have demonstrated for the first time in this study that, in glioblastoma CSLCs, FoxO3a has a "negative" role in the maintenance of stem cell-like properties. This finding may be in line with the recent observation that FoxO3a expression in human glioma samples is correlated with the malignant grade and that low FoxO3a expression is associated with poor patient outcome [22]. Of note, conversely, high expression of FoxO3a has been reported to be associated with a poor prognosis in acute myeloid leukemia [23], in agreement with its "positive" role in the maintenance of stem cell-like properties in LICs, again underscoring the different roles of FoxO3a in different cancer types. The opposite roles of FoxO3a in these two different cancer types may be reflected by the fact that LICs display a quiescent phenotype whereas glioblastoma CSLCs display a proliferative phenotype [21, 24]. At present, it remains totally unknown what underlies such heterogeneity of CSLCs, but identification of FoxO3a transcriptional targets involved in the control of each cancer type might provide clues to understand the underlying mechanism at the molecular level.

Strikingly, the function of FoxO3a in glioblastoma CSLCs was in sharp contrast to its function reported for neural stem cells [25]. Although FoxO3a function was required for the differentiation of glioblastoma CSLCs in our study, it was essential for the maintenance of neural stem cells in adult mice. Indeed, FoxO3a was active and localized in the nucleus in self-renewing neural stem cells, while it was active and localized in the nucleus in differentiated glioblastoma CSLCs. FoxO3a phosphorylation patterns were also highly contrasting: FoxO3a was phosphorylated by Akt in differentiated neural stem cells, whereas it was phosphorylated by Akt in

self-renewing glioblastoma CSLCs [25] (this study). These findings are rather surprising in that the same molecule functions in an entirely opposite manner in neural stem cells and glioblastoma CSLCs, which are generally presumed to share common mechanisms of regulation [26]. Although it currently remains unknown what causes this contrasting difference between neural stem cells and glioblastoma CSLCs in terms of FoxO3a function, it could be a great advantage when FoxO3a is considered as a therapeutic target (see below).

We found in this study that FoxO3a is required for the differentiation but not for the inhibition of self-renewal, both of which were induced by inhibition of the PI3K/Akt/mTOR and MEK/ERK pathways in glioblastoma CSLCs. This finding indicates that, under the control of the two signaling pathways, distinct molecular mechanisms govern the maintenance/loss of stem cell-like properties and the acquisition of differentiation phenotypes by glioblastoma CSLCs, the former being independent of and the latter being dependent on FoxO3a. Importantly, forced activation of FoxO3a not only induced the expression of differentiation markers but also subsequently inhibited stem/progenitor marker expression, and consequently the self-renewal capacity of glioblastoma CSLCs as indicated by decreased sphere formation. This suggests that FoxO3a may not be required for the initial loss of stem cell-like properties of glioblastoma CSLCs preceding the expression of differentiation markers but may contribute to ensuring and establishing a cellular condition in which cells can never restore the stem cell-like state. Therefore, it seems that the exact role of FoxO3a in glioblastoma CSLCs is to promote their "irreversible commitment" to differentiation. However, it is unlikely that FoxO3a is the sole transcription factor for the differentiation of glioblastoma CSLCs, because FoxO3a expression was not required for the differentiation of glioblastoma CSLC induced by serum. As the members of the FoxO family are known for their overlapping functions [19], it is possible that other FoxO family members, for instance FoxO1, might compensate for the lack of FoxO3a function to promote differentiation of glioblastoma CSLCs.

The results of this study suggest that, although they do not necessarily exclude the involvement of other redundant mechanisms as discussed above, FoxO3a is at least in part responsible for the inhibition of tumorigenic potential of glioblastoma CSLCs by combinational inhibition of the PI3K/Akt/mTOR and MEK/ERK pathways. These results give rise to a novel and important notion from a therapeutic perspective that any measures that activate FoxO3a would be sufficient to promote differentiation of glioblastoma CSLCs and thereby inhibit their self-renewal and tumorigenic potential. Indeed, we found in support of this notion that oxidative stress induced by H_2O_2 treatment effectively deprives glioblastoma CSLCs of their tumorigenic potential independently of the PI3K/Akt/mTOR and MEK/ERK pathways (Supplementary Information Fig. 8). To date, a number of other mechanisms have been reported to regulate FoxO3a. For example, IkappaB kinase (IKKβ) or serum-glucocorticoid-related kinases phosphorylate FoxO3a, which triggers nuclear export and cytoplasmic sequestration, thereby inhibiting access to DNA binding sites [27, 28]. Intriguingly, in the case of acute myeloid leukemia, IKKβ overcomes PI3K/Akt and ERK/MAPK to control FoxO3a activity, and blockade of the IKK/nuclear factor kappa B (NFκB) signaling pathway has already been proposed as a possible therapeutic strategy [29–31]. It has also been reported that metformin, which activates AMP-activated kinase (AMPK) by increasing the cellular AMP/ATP ratio, inhibits cancer cell growth and regulates FoxO3a through AMPK [32, 33]. Therefore, targeting these molecules involved in the regulation of FoxO3a function could be a potential and attractive way to control glioblastoma CSLCs. Significantly, the role of FoxO3a in glioblastoma CSLCs and adult neural stem cells appears to be entirely different as described above. Therefore, it might be possible to selectively inhibit the tumorigenicity of glioblastoma CSLCs while sparing the function of neural stem cells, making FoxO3a an ideal candidate of molecular targeting therapy.

Summary

In summary, we have disclosed in this study that FoxO3a is kept in check under the control of the PI3K/Akt/mTOR and MEK/ERK pathways to maintain the stem cell-like state of glioblastoma CSLCs and that unleashing FoxO3a from this restraint is sufficient to commit them to differentiation and suppress their tumorigenicity. These findings will contribute to the development of novel treatment strategies for glioblastoma.

Acknowledgments

We thank Dr. Kimishige Ishizaka for invaluable comments on the manuscript. This work was supported by Grants-in-Aid for Scientific Research, Challenging Exploratory Research, Young Scientists and for Scientific Research on Priority areas from the Ministry of Education, Culture, Sports, Science, and Technology of Japan; by a Grant-in-Aid from the Global COE program of the Japan Society for the Promotion of Science; by a Grant-in-Aid for Cancer Research from the Ministry of Health, Labor, and Welfare of Japan; and by a grant from the Japan Brain Foundation.

Disclosure of Potential Conflicts of Interest

The authors have no conflicts of interest to declare.

References

1 Stupp R, Mason WP, van den Bent MJ et al. Radiotherapy plus concomitant and adjuvant temozolomide for glioblastoma. N Engl J Med 2005;352:987–996.
2 Ignatova TN, Kukekov VG, Laywell ED et al. Human cortical glial tumors contain neural stem-like cells expressing astroglial and neuronal markers in vitro. Glia 2002;39:193–206.
3 Hemmati HD, Nakano I, Lazareff JA et al. Cancerous stem cells can arise from pediatric brain tumors. Proc Natl Acad Sci USA 2003;100:15178–15183.
4 Singh SK, Hawkins C, Clarke ID et al. Identification of human brain tumour initiating cells. Nature 2004;432:396–401.
5 Galli R, Binda E, Orfanelli U et al. Isolation and characterization of tumorigenic, stem-like neural precursors from human glioblastoma. Cancer Res 2004;64:7011–7021.
6 Park DM, Rich JN. Biology of glioma cancer stem cells. Mol Cells 2009;28:7–12.
7 Liu G, Yuan X, Zeng Z et al. Analysis of gene expression and chemoresistance of CD133+ cancer stem cells in glioblastoma. Mol Cancer 2006;5:67.
8 Blazek ER, Foutch JL, Maki G. Daoy medulloblastoma cells that express CD133 are radioresistant relative to CD133- cells, and the CD133+ sector is enlarged by hypoxia. Int J Radiat Oncol Biol Phys 2007;67:1–5.
9 Frank NY, Schatton T, Frank MH. The therapeutic promise of the cancer stem cell concept. J Clin Invest 2010;120:41–50.
10 Piccirillo SG, Reynolds BA, Zanetti N et al. Bone morphogenetic proteins inhibit the tumorigenic potential of human brain tumour-initiating cells. Nature 2006;444:761–765.

11 Ikushima H, Todo T, Ino Y et al. Autocrine TGF-beta signaling maintains tumorigenicity of glioma-initiating cells through Sry-related HMG-box factors. Cell Stem Cell 2009;5:504–514.
12 Wurdak H, Zhu S, Romero A et al. An RNAi screen identifies TRRAP as a regulator of brain tumor-initiating cell differentiation. Cell Stem Cell 2010;6:37–47.
13 Zheng H, Ying H, Wiedemeyer R et al. PLAGL2 regulates Wnt signaling to impede differentiation in neural stem cells and gliomas. Cancer Cell 2010;17:497–509.
14 Sunayama J, Matsuda KI, Sato A et al. Crosstalk between the PI3K/mTOR and MEK/ERK pathways involved in the maintenance of self-renewal and tumorigenicity of glioblastoma stem-like cells. Stem Cells 2010;28:1930–1939.
15 Sunayama J, Sato A, Matsuda KI et al. Dual blocking of mTor and PI3K elicits a prodifferentiation effect on glioblastoma stem-like cells. Neuro Oncol 2010;12:1205–1219.
16 Brunet A, Bonni A, Zigmond MJ et al. Akt promotes cell survival by phosphorylating and inhibiting a forkhead transcription factor. Cell 1999;96:857–868.
17 Yang JY, Zong CS, Xia W et al. ERK promotes tumorigenesis by inhibiting FOXO3a via MDM2-mediated degradation. Nat Cell Biol 2008;10:138–148.
18 Skurk C, Maatz H, Kim HS et al. The Akt-regulated forkhead transcription factor FOXO3a controls endothelial cell viability through modulation of the caspase-8 inhibitor FLIP. J Biol Chem 2004;279:1513–1525.
19 Yang JY, Hung MC. A new fork for clinical application: targeting forkhead transcription factors in cancer. Clin Cancer Res 2009;15:752–757.
20 Dubrovska A, Kim S, Salamone RJ et al. The role of PTEN/Akt/PI3K signaling in the maintenance and viability of prostate cancer stem-like cell populations. Proc Natl Acad Sci USA 2009;106:268–273.
21 Naka K, Hoshii T, Muraguchi T et al. TGF-beta-FOXO signalling maintains leukaemia-initiating cells in chronic myeloid leukaemia. Nature 2010;463:676–680.
22 Shi J, Zhang L, Shen A et al. Clinical and biological significance of forkhead class box O 3a expression in glioma: mediation of glioma malignancy by transcriptional regulation of p27kip1. J Neurooncol 2010;98:57–69.
23 Santamaria CM, Chillon MC, Garcia-Sanz R et al. High FOXO3a expression is associated with a poorer prognosis in AML with normal cytogenetics. Leuk Res 2009;33:1706–1709.
24 Lathia JD, Gallagher J, Heddleston JM et al. Integrin alpha 6 regulates glioblastoma stem cells. Cell Stem Cell 2010;6:421–432.
25 Renault VM, Rafalski VA, Morgan AA et al. FoxO3 regulates neural stem cell homeostasis. Cell Stem Cell 2009;5:527–539.
26 Stiles CD, Rowitch DH. Glioma stem cells: a midterm exam. Neuron 2008;58:832–846.
27 Hu MC, Lee DF, Xia W et al. IkappaB kinase promotes tumorigenesis through inhibition of forkhead FOXO3a. Cell 2004;117:225–237.
28 Leong ML, Maiyar AC, Kim B et al. Expression of the serum- and glucocorticoid-inducible protein kinase, Sgk, is a cell survival response to multiple types of environmental stress stimuli in mammary epithelial cells. J Biol Chem 2003;278:5871–5882.
29 Chapuis N, Park S, Leotoing L et al. I{kappa}B kinase overcomes PI3K/Akt and ERK/MAPK to control FOXO3a activity in acute myeloid leukemia. Blood 2010;116:4240–4250.
30 Frelin C, Imbert V, Griessinger E et al. Targeting NF-kappaB activation via pharmacologic inhibition of IKK2-induced apoptosis of human acute myeloid leukemia cells. Blood 2005;105:804–811.
31 Carvalho G, Fabre C, Braun T et al. Inhibition of NEMO, the regulatory subunit of the IKK complex, induces apoptosis in high-risk myelodysplastic syndrome and acute myeloid leukemia. Oncogene 2007;26:2299–2307.
32 Zakikhani M, Dowling R, Fantus IG et al. Metformin is an AMP kinase-dependent growth inhibitor for breast cancer cells. Cancer Res 2006;66:10269–10273.
33 Canto C, Gerhart-Hines Z, Feige JN et al. AMPK regulates energy expenditure by modulating NAD+ metabolism and SIRT1 activity. Nature 2009;458:1056–1060.


See www.StemCells.com for supporting information available online.

Int. J. Radiation Oncology Biol. Phys., Vol. 81, No. 4, pp. e475–e480, 2011

0360-3016/$ - see front matter

ELSEVIER

doi:10.1016/j.ijrobp.2011.02.016

CLINICAL INVESTIGATION Brain

COMPARISON OF CLINICAL OUTCOMES OF SURGERY FOLLOWED BY LOCAL BRAIN RADIOTHERAPY AND SURGERY FOLLOWED BY WHOLE BRAIN RADIOTHERAPY IN PATIENTS WITH SINGLE BRAIN METASTASIS: SINGLE-CENTER RETROSPECTIVE ANALYSIS

KENJI HASHIMOTO, M.D.,* YOSHITAKA NARITA, M.D.,* YASUJI MIYAKITA, M.D.,* MAKOTO OHNO, M,D.,* MINAKO SUMI, M.D.,† HIROSHI MAYAHARA, M.D.,† TAKAMASA KAYAMA, M.D.,* AND SOICHIRO SHIBUI, M.D.*

Divisions of *Neurosurgery and †Radiation Oncology, National Cancer Center Hospital, Tokyo, Japan

Purpose: Data comparing the clinical outcomes of local brain radiotherapy (LBRT) and whole brain RT (WBRT) in patients with a single brain metastasis after tumor removal are limited.

Patients and Methods: A retrospective analysis was performed to compare the patterns of treatment failure, cause of death, progression-free survival, median survival time, and Karnofsky performance status for long-term survivors among patients who underwent surgery followed by either LBRT or WBRT between 1990 and 2008 at the National Cancer Center Hospital.

Results: A total of 130 consecutive patients were identified. The median progression-free survival period among the patients who received postoperative LBRT ($n = 64$) and WBRT ($n = 66$) was 9.7 and 11.5 months, respectively ($p = .75$). The local recurrence rates (LBRT, 9.4% vs. WBRT, 12.1%) and intracranial new metastasis rate (LBRT, 42.2% vs. WBRT, 33.3%) were similar in each arm. The incidence of leptomeningeal metastasis was also equivalent (LBRT, 9.4% vs. WBRT, 10.6%). The median survival time for the LBRT and WBRT patients was 13.9 and 16.7 months, respectively ($p = .88$). A neurologic cause of death was noted in 35.6% of the patients in the LBRT group and 36.7% of the WBRT group ($p = .99$). The Karnofsky performance status at 2 years was comparable between the two groups.

Conclusions: The clinical outcomes of LBRT and WBRT were similar. A prospective evaluation is warranted.

Local brain radiotherapy, Whole brain radiotherapy, Single brain metastasis, Clinical outcomes, Long-term result.

INTRODUCTION

Whole brain radiotherapy (WBRT) has served as the standard of care for patients with brain metastases worldwide (1, 2). In patients with a single brain metastasis, postoperative WBRT has demonstrated better intracranial tumor control for both surgical lesions and nonsurgical new lesions and a lower rate of a neurologic cause of death compared with surgery alone (3). However, the addition of WBRT did not result in a survival benefit or extend the duration of the interval that the patients remained functionally independent. Some prospective trials, with the exception of one, and pooled analyses have clarified that a survival benefit for surgery followed by WBRT does exist compared with WBRT alone (1, 4–7). Other studies have also revealed that surgery followed by WBRT increased the duration of neurocognitive functional independence, as well as intracranial tumor control (4–6, 8, 9). Accordingly, surgery followed by WBRT has been the standard of care for patients with a single brain metastasis.

The median survival time of patients with brain metastases is considered to be approximately 2–7 months; favorable and unfavorable subgroups can be classified using recursive partitioning analysis (RPA) (10). However, about 2–8% of patients with brain metastasis can achieve longer survival periods (11, 12). Delayed WBRT toxicity, hypopituitarism, dementia, and memory disturbances influencing cognitive function have also been discussed, although the primary brain lesion is mainly responsible for the deterioration of functional independence (11, 13, 14).

Because WBRT is widely believed to induce dementia in patients with brain metastases, local brain RT (LBRT) as a substitute for WBRT has been widely accepted in some

Reprints requests to: Yoshitaka Narita, M.D., Division of Neurosurgery, National Cancer Center Hospital, 5-1-1 Tsukiji, Chuo-ku, Tokyo 104-0045 Japan. Tel: (+81) 3-3542-2511; Fax: (+81) 3-3542-3815; E-mail: yonarita@ncc.go.jp

Conflict of interest: none.

Received Sept 24, 2010, and in revised form Jan 28, 2011. Accepted for publication Feb 2, 2011.

Table 1. Patient characteristics (n = 130)

Characteristic	All patients	Range	LBRT (n = 64)	WBRT (n = 66)	p
Age (y)	58	24–87	58 (38–87)	58 (24–79)	.35
Karnofsky performance status	70	40–100	70 (40–100)	70 (40–100)	.35
RPA class	II	I–III	II (I–III)	II (I–III)	.78*
I	40	30.8	19	21	
II	55	42.3	26	29	
III	35	26.9	19	16	
Cancer type (%)					.96*
Lung cancer	55	42.3	29	26	
Non–small-cell lung cancer	54		29	25	
Small-cell lung cancer	1		0	1	
Breast cancer	18	13.8	9	9	
Colorectal cancer	14	10.8	6	8	
Skin cancer	6	4.6	3	3	
Other	37	28.5	17	20	
Diameter of brain tumor (mm)	38	10–65	38 (10–65)	38 (15–60)	.57
Removal status					.11
Gross total removal	124	95.4	59	65	
Partial removal	6	4.6	5	1	

Abbreviations: RPA = recursive partitioning analysis; WBRT = whole brain radiotherapy; LBRT = local brain radiotherapy,
Data presented as median, with range in parentheses.
* Chi-square test.

institutions in Japan (15). LBRT delivered by linear accelerator to the tumor bed with a margin determined using the two-field technique (opposing portal irradiation) according to a dose-fractionated schedule had been applied for the treatment of single brain metastasis after surgical removal at the National Cancer Center Hospital before September 2004. This was based on the ethics that we presumed we could treat intracranial relapse using stereotactic RT after LBRT. After discussion with neurosurgeons, radio-oncologists, and medical oncologists, however, the treatment policy was changed. WBRT has been used for the treatment of all patients with single brain metastasis after tumor removal since October 2004. A Phase I-II clinical trial of postoperative LBRT was reported, and the investigators concluded that LBRT was not a suitable substitute for WBRT (16). However, that previous study included only 12 patients, and 7 of these patients died of intracranial tumor progression. The median survival time was 7.2 months, similar to that after WBRT. Another retrospective study implied that LBRT might have a similar benefit to that of WBRT in patients with a single brain metastasis (17). Bahl *et al.* (18) reported 7 cases of postoperative LBRT, of which 4 cases recurred at the same site. These studies included only a small number of patients, and any conclusions regarding the clinical outcome of postoperative LBRT, especially compared with that of postoperative WBRT, are thus difficult to make. In the present analysis, we retrospectively compared the clinical outcomes of patients with a single brain metastasis who received surgery followed by either WBRT or LBRT.

PATIENTS AND METHODS

Patient population

From the database of the neurosurgery division at the National Cancer Center Hospital, we identified patients who had undergone brain tumor removal followed by RT between 1990 and 2008. The patients were included in the present analysis if they met the following criteria: age ≥18 years, a single brain metastasis identified by magnetic resonance imaging, and tumor removal followed by either WBRT or LBRT. The exclusion criteria were as follows: extracranial malignant lymphoma or hematological tumor; brain biopsy only; previous brain RT; surgery followed by observation, with brain RT once progression was recognized; and postoperative gamma knife or linear accelerator-based radiosurgery. All the patients who received LBRT (n = 64) were treated before October 2004, and all the patients who received WBRT (n = 66) were treated after October 2004.

Data collection and definitions of terms

All the medical charts for the eligible patients were reviewed. To compare the clinical outcomes of postoperative WBRT and LBRT, we collected the following data:; preoperative magnetic resonance imaging; date of surgery and RT; RPA classification before surgery; Karnofsky performance status (KPS) at presentation; primary tumor site; date of recognition of local recurrence or intracranial new metastases; patterns of progression; leptomeningeal metastasis development; date of death; and neurologic cause of death. For the additional evaluation of long-term survivors (≥2 years after surgery), we also reviewed the KPS at 2 years after surgery.

Local recurrence was defined as recurrence at the surgical site. Intracranial new metastases included the detection of new brain metastases other than those occurring at the surgical site or the development of leptomeningeal metastases. Leptomeningeal metastases were diagnosed using a cytologic examination of cerebrospinal fluid.

Surgery and RT

The surgical indications for single brain metastasis were generally as follows: tumor diameter ≥30 mm or a tumor diameter of <30 mm with neurologic dysfunction.

Whole brain RT was administered through two lateral ports covering the brain and meninges to the foramen magnum. Normally, WBRT was delivered using a 4-MV or 6-MV linear accelerator at

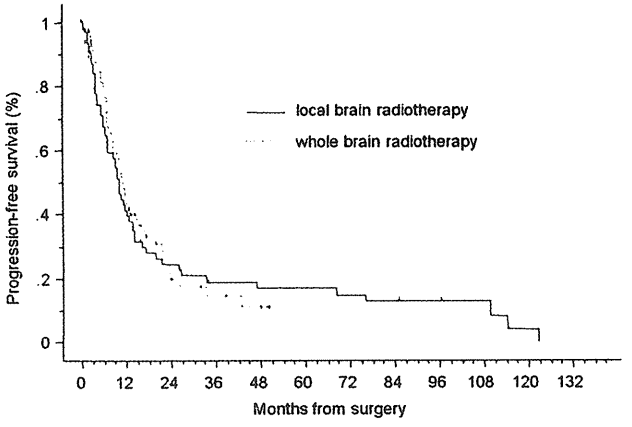

Fig. 1. Progression-free survival for patients with local brain radiotherapy (black line) and whole brain radiotherapy (dashed line).

a total dose of 30 Gy in 10 fractions or 37.5 Gy in 15 fractions. Patients who received LBRT underwent computed tomography simulation in the supine position. The clinical target volume consisted of the tumor cavity plus a 1.5-cm margin, and the planning target volume was created by expanding the clinical target volume by 0.5 cm. LBRT was administered using a 6-MV linear accelerator to the tumor bed using a two-field technique according to a dose-fractionated schedule. Normally, LBRT was delivered at a total dose of 50 Gy in 25 fractions.

Statistical analysis

Postoperative differences in local recurrence, intracranial new metastases, the development of leptomeningeal metastases, and neurologic cause of death were compared between the WBRT and LBRT groups using the Fisher exact test. Numeric data, including RPA, KPS, and age, were compared using the Mann-Whitney *U* test. Progression-free survival was defined as the interval between the date of surgery to the date of the recognition of local recurrence or intracranial new metastases. Death was treated as an event, and the absence of disease progression was treated as a censored observation on the last day of follow-up. Overall survival was defined as the interval from the date of surgery to the date of death. Patients who were lost to follow-up were treated as a censored observation on the last day of follow-up. Univariate and multivariate analyses using the Cox proportional hazard model were performed to identify relevant factors affecting survival. The numeric factors analyzed in the Cox analyses were dichotomized according to the median number. All statistical analyses were performed using StatView, version 5.0 (SAS Institute, Tokyo, Japan).

RESULTS

Of the 421 surgical cases, we identified 130 patients who met the eligibility criteria. The characteristics of these patients are listed in Table 1. Of the 130 patients, 66 had received postoperative WBRT and 64 had received postoperative LBRT. Of the 66 patients who had received WBRT, 34 (51.5%) were treated to a dose of 30 Gy delivered in 10 fractions, and 31 (47.0%) were treated to a dose of 37.5 Gy delivered in 15 fractions. Of the 64 patients who received LBRT, 57 (89.1%) were treated to a dose of 50 Gy in 25 fractions, and 7 were treated with a variety of dose-fractionation schedules (24 Gy in 12 fractions to 60 Gy in 30 fractions).

The median progression-free survival period for the patients who received postoperative LBRT and WBRT was 9.7 and 11.5 months, respectively ($p = .75$; Fig. 1). The patients who underwent LBRT and WBRT developed 33 and 30 recurrences, respectively. The local recurrence rates (9.4% vs. 12.1%) and intracranial new metastases rates (42.2% vs. 33.3%) were not significantly different between the LBRT and WBRT groups (Table 2). The incidence of leptomeningeal metastases in patients receiving LBRT and WBRT was 9.4% and 10.6%, respectively ($p = .99$).

The median survival time for patients who received postoperative LBRT and WBRT was 13.9 and 16.7 months, respectively ($p = .88$; Fig. 2). Of the 64 patients who received LBRT and the 66 patients who received and WBRT, 59 and 49 died, respectively. A neurologic cause of death was noted in 35.6% of the patients in the LBRT group and 36.7% of the patients in the WBRT group ($p = .99$; Table 2). Univariate analyses revealed that only the RPA classification correlated significantly with survival (hazard ratio [HR], 0.436; $p = .002$). In particular, RT (LBRT vs. WBRT) did not correlate with survival (HR, 1.031; $p = .88$; Table 3). Multivariate analyses revealed that RPA was the only significant factor associated with survival (HR, 0.399; $p = .001$). Neither LBRT nor WBRT was related to survival (HR, 0.933; $p = .74$; Table 4).

Table 2. Patterns of treatment failure in patients who received WBRT and LBRT

Variable	LBRT ($n = 64$)	WBRT ($n = 66$)	
Total recurrences identified *(n)*	33	30	*p*
Local recurrence	6 (18.2)	8 (26.7)	.61
Distant metastasis	27 (81.8)	22 (73.3)	.61
Development of leptomeningeal metastases *(n)*	6	7	.99
Total deaths identified *(n)*	59	49	
Neurologic cause of death	21 (35.6)	18 (36.7)	.98*
Other	21 (35.6)	17 (34.7)	
Unknown	17 (28.8)	15 (30.6)	

Abbreviations: WBRT = whole brain radiotherapy; LBRT = local brain radiotherapy.
Data in parentheses are percentages.
* Chi-square test.

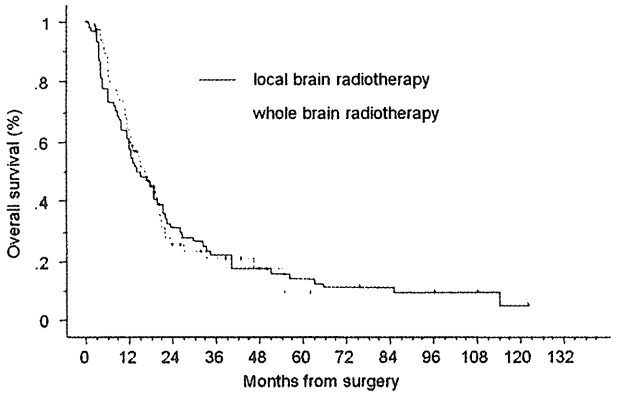

Fig. 2. Overall survival in patients with local brain radiotherapy (black line) and whole brain radiotherapy (dashed line).

We further analyzed the patterns of RT after recurrence in patients who received either postoperative LBRT or WBRT. Of the 33 patients who developed recurrences after postoperative LBRT, additional RT was performed in 15 (45.5%). Of the 15 patients, 6 underwent gamma knife or linear accelerator-based radiosurgery. LBRT was performed in 5 patients, and 4 received WBRT. Of the 30 patients who developed recurrences after postoperative WBRT, 16 (53.3%) received additional RT. Of the 16 patients, 13 received gamma knife or linear accelerator-based radiosurgery, and 3 received LBRT.

Among the patients who survived for >2 years, we compared the KPS at 2 years after surgery. A total of 20 patients who had received postoperative LBRT and 13 who had received postoperative WBRT were identified. The median KPS score at 2 years for these patients in the LBRT and WBRT groups was 80 (range, 60–100) and 80 (range, 60–100; $p = .99$), respectively. Of the 20 patients who had received LBRT, 9 experienced relapse in a local lesion, 2 had focal signs without relapse, which might have indicated radiation necrosis, and 7 had been well without relapse. For 2 other patients, this information was not available.

DISCUSSION

We have revealed the clinical outcomes of postoperative LBRT among patients with single metastasis and compared them with those of patients who underwent postoperative WBRT. The clinical outcomes, including progression-free survival, overall survival, local recurrence, intracranial new metastases, development of leptomeningeal metastases, and neurologic cause of death, were not significantly different between the two groups. In an analysis of relapse patterns, the patients treated with LBRT tended to have a lower probability of developing local recurrence (9.4% vs. 12.1%) and a greater probability of developing intracranial new metastases (42.2% vs. 33.3%), although these values were not significantly different. The probability of developing leptomeningeal metastases was also similar in each group (9.4% vs. 10.6%).

Previous reports have indicated that the addition of WBRT after tumor removal significantly reduces the local recurrence rate (3, 9). However, approximately 6–50% of patients develop relapses at new intracranial sites in the brain (5, 9, 19). Furthermore, about 20–30% of patients with brain metastasis die of neurologic causes even if a radiation boost has been added using stereotactic radiosurgery to increase local control, although the presence of extracranial lesions is the strongest factor for predicting survival (7, 20, 21). In our study, intracranial new metastases were predominant in both groups. The frequency of intracranial recurrence (new local and intracranial metastases) was somewhat greater than in previous series, although the rate of a neurologic cause of death was equivalent. Importantly, the patterns of treatment failure were similar in the LBRT and WBRT groups. Muacevic *et al.* (22) insisted that postoperative WBRT should be applied in patients with a single brain metastasis to destroy so-called micrometastases, based on the results of their randomized trial. They compared patients with a small single metastasis who received either surgery plus WBRT or gamma knife surgery alone. Their sample size was underpowered, although the risk of intracranial new metastases seemed to be lower in the WBRT cohort. To date, no randomized trials comparing the clinical outcomes of postoperative WBRT and postoperative gamma knife or linear accelerator-based radiosurgery, or LBRT have been reported.

We have demonstrated a similar efficacy for LBRT and WBRT. WBRT has problems in terms of delayed toxicity developing leukoencephalopathy, although the number of long-term survivors with brain metastasis seems to be somewhat low (11, 12). LBRT might be beneficial with regard to the protection of normal brain tissue. We compared the KPS

Table 3. Univariate analyses regarding survival

Variable	HR	95% CI	*p*
RT (LBRT vs. WBRT)	1.031	0.698–1.523	.88
RPA classification			
I vs. III	0.436	0.259–0.733	.002
II vs. III	0.808	0.514–0.127	.35
Removal status (gross total removal vs. partial removal)	0.948	0.385–2.334	.91
Tumor diameter (≥38 vs. <38 mm)	1.053	0.718–1.543	.79
Cancer type (lung cancer vs. other)	0.694	0.470–1.025	.062

Abbreviations: RT = radiotherapy; HR = hazard ratio; CI = confidence interval; other abbreviations as in Table 1.

Table 4. Multivariate analyses regarding survival

Variable	HR	95% CI	*p*
RT (LBRT vs. WBRT)	0.933	0.614–1.416	.743
RPA classification			
I vs. III	0.399	0.232–0.688	.001
II vs. III	0.736	0.455–1.191	.22
Removal status (gross total removal vs. partial removal)	0.622	0.239–1.615	.33
Tumor diameter (≥38 vs. <38 mm)	0.852	0.559–1.297	.45
Cancer type (lung cancer vs. other)	0.662	0.438–1.001	.05

Abbreviations as in Tables 1 and 3.

at 2 years to examine any delayed toxicity. Because of the nature of the present retrospective study, the detailed neurocognitive function or quality of life of the patients could not be identified. Among the long-term survivors, however, the KPS was preserved in both treatment groups. Thus, LBRT might be indicated for elderly patients at risk of developing dementia if LBRT has the same ability to control primary brain tumors, which is considered to be the main factor affecting neurocognitive function (14).

The present study had some limitations because of its retrospective nature. First, the radiation dose varied. About 90% of the LBRT patients received a dose of 50 Gy delivered in 25 fractions, and approximately 50% of the WBRT patients received a dose of 30 Gy delivered in 10 fractions; the others received a dose of 37.5 Gy delivered in 15 fractions. According to the summary by Tsao *et al.* (1), no differences in terms of survival or neurocognitive function were observed among the various dose-fraction schedules of WBRT. Second, the present study was a historical case-control study comparing LBRT and WBRT. Patients at risk of developing multiple metastases might have undergone WBRT during the period before 2004, when we started performing WBRT as the standard of care. Thus, the patients who were treated with LBRT might have had better general condition compared with the patients who were treated with WBRT. We compared the baseline characteristics of each treatment arm and used multivariate analyses to reduce any potential biases.

CONCLUSIONS

We have demonstrated the clinical efficacy of LBRT compared with WBRT on a large scale. The clinical outcomes, including progression-free survival, overall survival, patterns of treatment failure, development of leptomeningeal metastases, and a neurologic cause of death, were similar in both treatment groups. The KPS at 2 years was also similar when the two groups were compared. This result should be evaluated in a prospective manner.

REFERENCES

1. Tsao MN, Lloyd NS, Wong RK, *et al.* Radiotherapeutic management of brain metastases: A systematic review and meta-analysis. *Cancer Treat Rev* 2005;31:256–273.
2. Coia LR. The role of radiation therapy in the treatment of brain metastases. *Int J Radiat Oncol Biol Phys* 1992;23: 229–238.
3. Patchell RA, Tibbs PA, Regine WF, *et al.* Postoperative radiotherapy in the treatment of single metastases to the brain: A randomized trial. *JAMA* 1998;280:1485–1489.
4. Noordijk EM, Vecht CJ, Haaxma-Reiche H, *et al.* The choice of treatment of single brain metastasis should be based on extracranial tumor activity and age. *Int J Radiat Oncol Biol Phys* 1994;29:711–717.
5. Patchell RA, Tibbs PA, Walsh JW, *et al.* A randomized trial of surgery in the treatment of single metastases to the brain. *N Engl J Med* 1990;322:494–500.
6. Vecht CJ, Haaxma-Reiche H, Noordijk EM, *et al.* Treatment of single brain metastasis: Radiotherapy alone or combined with neurosurgery? *Ann Neurol* 1993;33:583–590.
7. Mintz AH, Kestle J, Rathbone MP, *et al.* A randomized trial to assess the efficacy of surgery in addition to radiotherapy in patients with a single cerebral metastasis. *Cancer* 1996;78:1470–1476.
8. Rades D, Fehlauer F, Schild S, *et al.* [Treatment for central neurocytoma: A meta-analysis based on the data of 358 patients]. *Strahlenther Onkol* 2003;179:213–218.
9. Nieder C, Astner ST, Grosu AL, *et al.* The role of postoperative radiotherapy after resection of a single brain metastasis: Combined analysis of 643 patients. *Strahlenther Onkol* 2007;183: 576–580.
10. Gaspar L, Scott C, Rotman M, *et al.* Recursive partitioning analysis (RPA) of prognostic factors in three Radiation Therapy Oncology Group (RTOG) brain metastases trials. *Int J Radiat Oncol Biol Phys* 1997;37:745–751.
11. Chao ST, Barnett GH, Liu SW, *et al.* Five-year survivors of brain metastases: A single-institution report of 32 patients. *Int J Radiat Oncol Biol Phys* 2006;66:801–809.
12. Lutterbach J, Bartelt S, Ostertag C. Long-term survival in patients with brain metastases. *J Cancer Res Clin Oncol* 2002; 128:417–425.
13. Sheline GE, Wara WM, Smith V. Therapeutic irradiation and brain injury. *Int J Radiat Oncol Biol Phys* 1980;6: 1215–1228.
14. Aoyama H, Tago M, Kato N, *et al.* Neurocognitive function of patients with brain metastasis who received either whole brain radiotherapy plus stereotactic radiosurgery or radiosurgery alone. *Int J Radiat Oncol Biol Phys* 2007;68:1388–1395.
15. Ueki K, Matsutani M, Nakamura O, *et al.* Comparison of whole brain radiation therapy and locally limited radiation therapy in the treatment of solitary brain metastases from non-small cell lung cancer. *Neurol Med Chir (Tokyo)* 1996;36:364–369.

16. Coucke PA, Zouhair A, Ozsahin M, *et al.* Focalized external radiotherapy for resected solitary brain metastasis: Does the dogma stand? *Radiother Oncol* 1998;47:99–101.
17. Iwadate Y, Namba H, Yamaura A. Whole-brain radiation therapy is not beneficial as an adjuvant therapy for brain metastases compared with localized irradiation. *Anticancer Res* 2002;22: 325–330.
18. Bahl G, White G, Alksne J, *et al.* Focal radiation therapy of brain metastases after complete surgical resection. *Med Oncol* 2006;23:317–324.
19. Smalley SR, Schray MF, Laws ER Jr., *et al.* Adjuvant radiation therapy after surgical resection of solitary brain metastasis: Association with pattern of failure and survival. *Int J Radiat Oncol Biol Phys* 1987;13:1611–1616.
20. Andrews DW, Scott CB, Sperduto PW, *et al.* Whole brain radiation therapy with or without stereotactic radiosurgery boost for patients with one to three brain metastases: Phase III results of the RTOG 9508 randomised trial. *Lancet* 2004;363:1665–1672.
21. Aoyama H, Shirato H, Tago M, *et al.* Stereotactic radiosurgery plus whole-brain radiation therapy vs stereotactic radiosurgery alone for treatment of brain metastases: A randomized controlled trial. *JAMA* 2006;295:2483–2491.
22. Muacevic A, Wowra B, Siefert A, *et al.* Microsurgery plus whole brain irradiation versus gamma knife surgery alone for treatment of single metastases to the brain: A randomized controlled multicentre phase III trial. *J Neurooncol* 2008;87:299–307.

J Neurooncol (2011) 103:619–627
DOI 10.1007/s11060-010-0433-0

CLINICAL STUDY – PATIENT STUDY

Prediction of malignancy grading using computed tomography perfusion imaging in nonenhancing supratentorial gliomas

Takaaki Beppu · Makoto Sasaki · Kohsuke Kudo · Akira Kurose · Masaru Takeda · Hiroshi Kashimura · Akira Ogawa · Kuniaki Ogasawara

Received: 10 June 2010 / Accepted: 20 September 2010 / Published online: 15 October 2010

Abstract Tumor grade differentiation is often difficult using routine neuroimaging alone. Computed tomography perfusion imaging (CTP) provides quantitative information on tumor vasculature that closely parallels the degree of tumor malignancy. This study examined whether CTP is useful for preoperatively predicting the grade of malignancy in glioma showing no enhancement on contrast-enhanced magnetic resonance imaging (MRI). Subjects comprised 17 patients with supratentorial glioma without enhancement on MRI. CTP was performed preoperatively, and absolute values and normalized ratios of parameters were calculated. Postoperatively, subjects were classified into two groups according to histological diagnosis of grade 3 (G3) glioma or grade 2 (G2) glioma. Absolute values and normalized ratios for each parameter were compared between G3 and G2. Accuracies of normalized ratios for cerebral blood flow (*n*CBF) and cerebral blood volume (*n*CBV) in predicting a diagnosis of G3 were assessed. In addition, *n*CBV was compared between diffuse astrocytoma, G2 oligodendroglial tumor (OT), and G3 OT. Values for *n*CBF and *n*CBV differed significantly between G3 and G2. Using *n*CBV of 1.6 as a cutoff, specificity and sensitivity for distinguishing G3 were 83.3% and 90.9%, respectively. No significant difference in *n*CBV was seen between diffuse astrocytoma and G2 OT, whereas differences were noted between G2 and G3 OTs, and between diffuse astrocytoma and G3 OT. CTP offers a useful method for differentiating between G3 and G2 in nonenhancing gliomas.

Keywords Computed tomography perfusion imaging · Diffuse astrocytoma · Glioma · Nonenhancement · Oligodendroglioma · Preoperative diagnosis

T. Beppu (✉) · M. Takeda · H. Kashimura · A. Ogawa · K. Ogasawara
Department of Neurosurgery, Iwate Medical University, Uchimaru 19-1, Morioka 020-8505, Japan
e-mail: tbeppu@iwate-med.ac.jp

M. Sasaki · K. Kudo
Advanced Medical Research Center, Iwate Medical University, Morioka, Japan

A. Kurose
Department of Pathology, Iwate Medical University, Morioka, Japan

Introduction

Glioma is graded according to World Health Organization (WHO) classification, with grade 1 or 2 graded as low-grade glioma (LGG) and grade 3 or 4 commonly defined as high-grade glioma (HGG) [1]. As treatment and prognosis differ substantially between LGG and HGG, the ability to differentiate between grade 2 (G2) glioma and grade 3 (G3) glioma, as the border between LGG and HGG, is very important. On contrast-enhanced computed tomography (CT) and magnetic resonance imaging (MRI), G2 gliomas are nonenhanced due to preservation of blood–brain barrier (BBB), whereas G3 gliomas are commonly enhanced due to increased vascular permeability caused by disruption of the BBB within the tumor [2–4]. However, the relationship between histological grading and contrast enhancement on CT and MRI is not always clear. Preoperatively differentiating between G3 and G2 gliomas that are nonenhanced on conventional neuroimaging is often difficult. When patients with nonenhancing glioma are encountered, neurooncologists may perform various examinations to differentiate between G3 and G2 gliomas, such as positron emission tomography (PET) for direct assessment of tumor

metabolism, magnetic resonance spectroscopy to detect magnetic resonance signals of metabolites, and diffusion-weighted MRI to clarify structures within and surrounding the tumor. Assessment of intratumoral vasculature is one approach that may help to clarify the intratumoral biological characteristics and malignancy of a tumor, as intratumoral angiogenesis and high vascularity, which are regulated by hypoxia and various vascular endothelial growth factors, are essential for tumor growth and progression [5–7].

Angiography enables direct observation of intratumoral vessels, but is hazardous and remains limited for depiction of intratumoral microvasculature. Magnetic resonance perfusion imaging (MRP) and CT perfusion imaging (CTP) provide reliable information on the intratumoral microvasculature [8–12]. Numerous studies of perfusion imaging have shown that increasing malignancy of the glioma is associated with increased intratumoral blood volume and vascular permeability [10, 13–15]. Quantitative evaluation from perfusion imaging thus depends on both the microvasculature (vascular density and diameter), and vascular permeability due to disruption or absence of the BBB within the tumor. Previous reports have shown good correlations between findings on perfusion imaging and malignancy grading in enhancing glioma. In contrast, the BBB of vessels is preserved in nonenhancing glioma, since extravasation of contrast medium through the BBB in tumor vessels is considered to represent the main cause of tumor contrast enhancement [4]. As MRI remains the preferred technique for assessing brain tumors, studies using MRP to thoroughly evaluate gliomas greatly outnumber those using CTP, and MRP has also been applied to neurooncological applications for nonenhancing gliomas, such as determining biopsy targets and predicting malignant progression [16–18]. In recent years, CTP has gained acceptance as a valuable imaging technique for assessing hemodynamics in brain tumors [13, 14, 19–22]. However, whether CTP is useful for grading malignancy of nonenhancing gliomas remains unclear. CTP retains the advantage of a linear relationship between attenuation changes on CT and tissue concentration of contrast medium, unlike MRP [8, 20]. We therefore hypothesized that CTP should accurately provide quantitative information on only the microvasculature within the tumor, excluding extravasation due to permeability, when limited to patients with nonenhancing glioma. In the present study, we performed CTP on patients with nonenhancing glioma, and compared cerebral blood volume (CBV), cerebral blood flow (CBF), and mean transit time (MTT), as quantitative values provided from CTP, with postoperative histological diagnosis. The present study aims to determine whether CTP is useful for prediction of preoperative malignancy grading (WHO G2 or G3) in nonenhancing glioma on contrast-enhanced MRI.

Patients and methods

Patients

The study protocol was approved by the Ethics Committee of Iwate Medical University, Morioka, Japan. Consecutive patients admitted to the Department of Neurosurgery at Iwate Medical University between September 2006 and January 2010 and meeting the entry criteria were recruited to this study. Entry criteria for this study comprised: diagnosis of supratentorial glioma; tumor bulk not clearly enhanced on gadolinium-enhanced T1-weighted MRI (Gd-T1WI); tumor bulk sited in the supratentorial cerebrum; no past history relating to the brain, including surgical operation, irradiation, administration of anticancer agents or steroids, stroke, infection, or other disorders such as demyelinating disease; and provision of written informed consent to participate. Subjects comprised 17 patients (7 men, 10 women) with mean age of 47.8 years. Patient data including age, tumor site, operation method, postoperative histological diagnosis, and malignancy grade are summarized in Table 1.

Table 1 Patient summary

No.	Age (years)	Tumor site	Surgery	Histology	WHO grade
1	76	Temporal lobe	Biopsy	AA	3
2	58	Frontal lobe	Resection	AO	3
3	45	Frontal lobe	Resection	AO	3
4	34	Frontal lobe	Resection	AO	3
5	29	Frontal lobe	Resection	AO	3
6	21	Frontal lobe	Resection	AOA	3
7	78	Frontal lobe	Biopsy	DA	2
8	68	Frontal lobe	Biopsy	DA	2
9	68	Parietal lobe	Biopsy	DA	2
10	65	Frontal lobe	Resection	DA	2
11	58	Frontal lobe	Resection	DA	2
12	52	Frontal lobe	Resection	Oli	2
13	46	Temporal lobe	Resection	Oli	2
14	42	Frontal lobe	Resection	OA	2
15	30	Frontal lobe	Resection	OA	2
16	27	Frontal lobe	Resection	DA	2
17	16	Temporal lobe	Resection	OA	2

AA anaplastic astrocytoma, *AO* anaplastic oligodendroglioma, *AOA* anaplastic oligoastrocytoma, *DA* diffuse astrocytoma, *Oli* oligodendroglioma, *OA* oligoastrocytoma

Conventional MRI and CTP

Conventional MRI was performed for all subjects within 7 days before surgery. Spin-echo Gd-T1WI was performed approximately 2 min after intravenous injection of gadolinium (0.2 ml/kg, Magnevist; Bayer Schering Pharma, Berlin, Germany), using a 3.0-T whole-body scanner (GE Yokogawa Medical Systems, Tokyo, Japan) with a standard head coil. We confirmed that the tumor in each patient did not show clear enhancement with gadolinium on Gd-T1WI.

CTP was also performed within 7 days before surgery using a 16-row multidetector CT system (Aquillion 16; Toshiba Medical Systems, Tokyo, Japan), in accordance with the methods described by Sasaki et al. [23]. After performing noncontrast CT to determine the location of the tumor balk, a multislice scan targeting the tumor bulk was performed (80 kV_p; 40 mA; 1.5 s/rotation, 30 rotations field of view, 240 × 240 mm^2; four contiguous 8-mm-thick sections; total scan time, 45 s). Five seconds after intravenously injecting 40 ml (4 ml/s) nonionic iodine contrast medium (Iopamiron 300; Bayer Schering Pharma) using a power injector, dynamic scanning was started and tissue attenuation of contrast medium was monitored on a slice. Radiation doses for the scanning protocol were as follows: volume CT dose index, 150 mGy; dose–length product, 480 mGy cm; and effective dose, 1.34 mSv. Data were transferred to a commercial workstation (M900 Quadra; Ziosoft, Tokyo, Japan), and scaled color maps for CBF, CBV, and MTT were automatically created. All mathematical analyses were performed by the deconvolution method [19, 24], using CTP analysis software supplied with the workstation described above. Among the three types of deconvolution algorithms implemented in this software, we used the block-circulant singular value decomposition method. Regions of interest (ROI) for venous output and arterial input functions were manually placed at the superior sagittal sinus and a single branch of the insular segment of the middle cerebral artery on either the pathological or nonpathological side, or A2 segment of the anterior cerebral artery, respectively. ROI were also placed over the entire tumor bulk and apparently normal white matter (ANWM) on the nonpathological side, on color maps for each parameter. Size of the ROI for ANWM was established as 1.0 cm^2. In the measurement of absolute values, the vascular-pixel elimination (VPE) method was used to exclude pixels from large vessels at the cerebral surface, sulci, and cisterns [23, 25]. In the present study, we established the VPE threshold as 6.0 ml/100 g for CBV, since high-CBV areas suggesting large cortical vessels on color map disappeared satisfactorily at 6.0 ml/100 g when the threshold was varied between 5.0 and 8.0 ml/100 g using our analysis software. Large vascular pixels were thus defined as pixels with CBV values >6.0 ml/100 g and were automatically eliminated. Regional absolute values (*r*CBF, *r*CBV, and *r*MTT) were then calculated automatically for all ROI. The measurements described above were performed twice for each patient by two investigators (M.S. and K.K.) who were blinded to all clinical data, including individual patient information and histological diagnosis. Absolute values of all parameters for each patient were determined as the mean of four measured values, as determined twice by each investigator. The second test was performed 1 week after the first test, with a different randomized order of measurements from the first test. We also calculated normalized ratios (*n*CBF, *n*CBV, and *n*MTT) as the absolute value for the tumor divided by the absolute value for the ANWM for each parameter in all patients. All patients underwent surgery, with tumor resection for 13 patients and CT-guided stereotactic needle biopsy for 4 patients (Table 1). The region targeted in stereotactic biopsy was based on findings from the CBV color map. If the color map showed heterogeneous perfusion within the tumor, the targeted region corresponded to the region with the highest perfusion area for CBV. In cases with tumor resection, histological diagnosis was determined by observation at the lesion showing the most malignant histological features in all preparations. Postoperatively, histological diagnosis using specimens obtained from surgery was made by one of the investigators (A.K.) with no prior knowledge of CTP data.

Statistical analyses

All data were analyzed using PASW Statistics version 18 software (SPSS Japan, Tokyo, Japan). Inter- and intrarater reliabilities for all absolute values were evaluated according to classification of the intraclass correlation coefficient (ICC) [26]. For $ICC_{(1,1)}$ and $ICC_{(1,k)}$ as interrater reliability, agreement of all absolute values (CBF, CBV, and MTT) between first and second tests was analyzed for tumor and ANWM for each investigator, using one-factor analysis of variance (ANOVA). For $ICC_{(2,1)}$ and $ICC_{(2,k)}$ as intrarater reliability, agreement of all absolute values between the two investigators was analyzed for tumor and ANWM for each test, using two-factor ANOVA. Patients were assigned to one of two histological grading groups according to histological classification: WHO G2 or WHO G3. Frequency of biopsy was compared between G2 and G3 groups using Fisher's exact probability test. We compared absolute values from the tumor lesion for each parameter between G2 and G3 using the Mann–Whitney *U* test. Furthermore, the normalized ratio for each parameter was compared between these groups again using the Mann–Whitney *U* test. The accuracy of *r*CBF and *n*CBV in predicting a diagnosis of G3 was assessed using receiver

operating characteristic (ROC) curves. ROC curves were calculated in increments of 0.1. Absolute values and normalized ratios for CBV were compared between diffuse astrocytoma, G2 oligodendroglial tumor (OT), and G3 OT, using the Mann–Whitney U test. G2 OTs comprised oligodendroglioma or oligoastrocytoma, whereas G3 OTs comprised anaplastic oligodendroglioma or anaplastic oligoastrocytoma. Statistical significance was established at the $P < 0.05$ level in all analyses.

Results

Based on histological diagnosis after surgery, 6 patients were assigned to the G3 group and 11 patients were assigned to the G2 group (Table 1). Of these 17 patients, 4 patients underwent stereotactic biopsy. Frequency of biopsy did not differ significantly between G3 and G2 groups ($P = 0.25$).

Interrater reliability was classified as "almost perfect" for both tumor and ANWM for each investigator: $ICC_{(1,1)}$ and $ICC_{(1,k)}$ for M.S. were 0.943 and 0.971 for tumor, and 0.961 and 0.980 for ANWM, respectively, and those for K.K. were 0.966 and 0.983 for tumor, and 0.942 and 0.970 for ANWM, respectively. Intrarater reliability was also classified as "almost perfect" for both tumor and ANWM in each test: $ICC_{(2,1)}$ and $ICC_{(2,k)}$ in the first test were 0.987 and 0.993 for tumor, and 0.973 and 0.987 for ANWM, respectively, and those in the second test were 0.971 and 0.985 for tumor, and 0.973 and 0.986 for ANWM, respectively. Absolute values of tumor lesions for each parameter in G3 and G2 groups are summarized in Table 2. Absolute values for all parameters varied widely, with no significant differences in any parameters identified between G3 and G2 groups. Normalized ratios for each parameter are summarized in Table 3. Significant differences between G3 and G2 groups were identified for nCBF and nCBV, with no significant differences in nMTT.

The cutoff for accuracy was defined as the point lying closest to the upper-left corner of the ROC curve.

Table 2 Absolute values for each parameter

	rCBF (ml/100 g/min)	rCBV (ml/100 g)	rMTT (s)
G3 ($n = 6$)			
Range	10.8–27.0	1.9–3.2	6.8–10.8
Mean ± SD	18.3 ± 5.3	2.5 ± 0.5	8.5 ± 1.5
G2 ($n = 11$)			
Range	8.8–23.3	1.3–2.6	7.0–12.2
Mean ± SD	15.5 ± 4.2	2.1 ± 0.4	8.8 ± 1.5
P	0.27	0.25	0.76

SD standard deviation

Table 3 Normalized ratios for each parameter

	nCBF	nCBV	nMTT
G3 ($n = 6$)			
Range	1.34–3.00	1.54–2.39	0.76–1.06
Mean ± SD	2.10 ± 0.57	1.92 ± 0.37	0.90 ± 0.12
G2 ($n = 11$)			
Range	0.92–2.00	0.91–1.75	0.79–1.07
Mean ± SD	1.41 ± 0.38	1.26 ± 0.28	0.91 ± 0.09
P	0.01	0.004	0.76

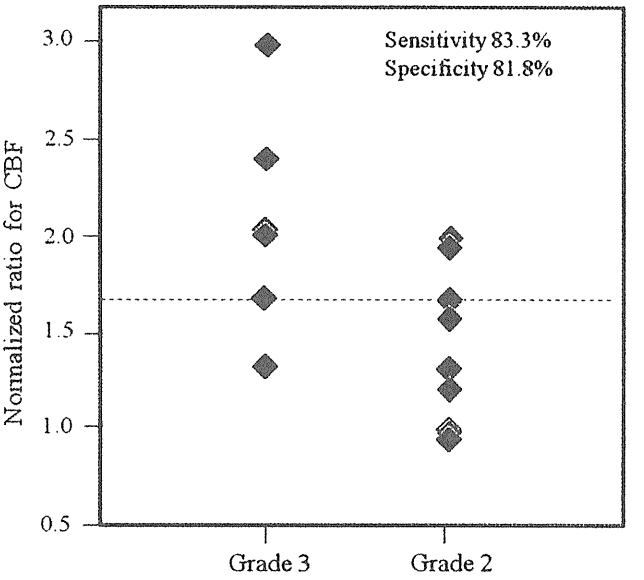

Fig. 1 Relationship between nCBF value and WHO grading. Using a cutoff of 1.7 (*dashed line*), nCBV was ≥1.7 for 5 (83.3%) of 6 patients with G3, compared with <1.7 for 9 (63.6%) of 11 patients with G2

Sensitivity and specificity in predicting a diagnosis of G3 were 83.3% and 81.8% for nCBF (cutoff 1.7), and 83.3% and 90.9% for nCBV (cutoff 1.6) (Figs. 1, 2). Accuracy for predicting a diagnosis of G3 was higher with nCBV than with nCBF.

A comparison of nCBV was made between G3 OT, G2 OT, and diffuse astrocytoma (Table 4). Significant differences in nCBV were identified between G3 and G2 OTs ($P = 0.009$), and between G3 OT and diffuse astrocytoma ($P = 0.02$), whereas no significant difference was seen between G2 OT and diffuse astrocytoma ($P = 0.36$).

Illustrative cases

We now describe the cases of two patients for whom CTP provided useful information for predicting tumor grading. Gd-T1WI for case 6 showed glioma with no clear enhancement in the right frontal lobe (Fig. 3a). Using the

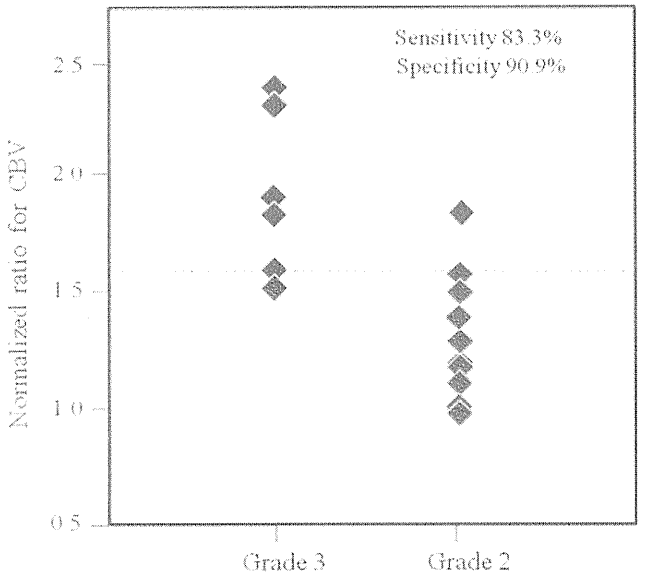

Fig. 2 Relationship between *n*CBV value and WHO grading. Using a cutoff point of 1.6 (*dashed line*), *n*CBV was ≥1.6 for 5 (83.3%) of 6 patients with G3 and <1.6 for 10 (90.9%) of 11 patients with G2

Table 4 Normalized ratio (mean ± SD) for CBV in G3 OT, G2 OT, and diffuse astrocytoma

	*n*CBV
G3 OT ($n = 5$)	1.99 ± 0.36
G2 OT ($n = 5$)	1.16 ± 0.24
Diffuse astrocytoma ($n = 6$)	1.35 ± 0.31

OT oligodendroglial tumors

VPE method, color mapping of CBV demonstrated large vessels of the cerebral surface to be successfully excluded (Fig. 3b). Color mapping of CBV depicted areas of hyperperfusion within the tumor. The *n*CBV for this case (*n*CBV = 2.3) was higher than the cutoff point. Tissue specimens obtained from gross total resection showed typical histological features of G3 anaplastic oligoastrocytoma.

Gd-T1WI for case 14 showed nonenhancing glioma of the right frontal lobe (Fig. 4a). The VPE method satisfactorily eliminated large vessels of the cerebral surface (Fig. 4b). On color mapping, areas of hyperperfusion seemed to be minor compared with those in case 6. The *n*CBV in this case (*n*CBV = 1.2) was lower than the cutoff point. After tumor resection, histological diagnosis was G2 oligoastrocytoma.

Discussion

Previous reports have documented that G3 gliomas make up 40–46% of nonenhancing gliomas on conventional MRI [3, 4]. Our finding of G3 tumors in 6 (35.2%) of 17 patients

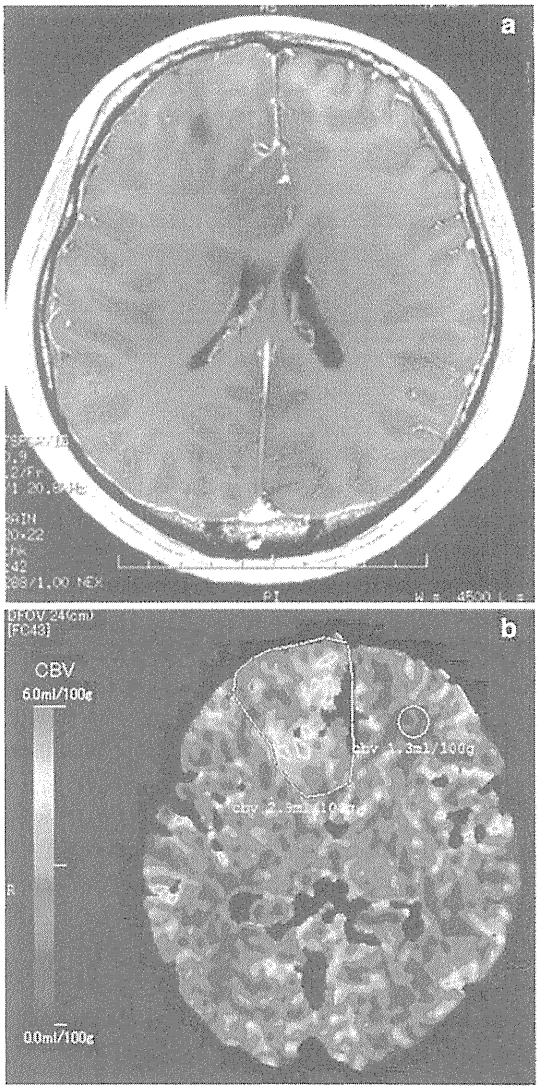

Fig. 3 Gd-T1WI (**a**) and color map of CBV (**b**) for case 6. *Circle* ROI covering the entire tumor bulk and ANWM localized on the nonpathological side

was close to this level. Thus, preoperative differentiation between G3 and G2 using MRI is often difficult. Biopsy or resection allowing histological diagnosis currently remain the basis for differentiation between G3 and G2 gliomas. However, neuroimaging can provide useful information on pathological diagnosis, particularly for patients who do not undergo biopsy or resection allowing histological diagnosis. Novel neuroimaging procedures other than routine MRI are thus desired. CTP and MRP provide reliable information on tumor vasculature, which can help to determine the extent of malignancy in glioma [8, 10, 22]. Although limitations of CTP include radiation dose and limited area of coverage compared with MRP, the linear relationship between attenuation changes on CT and tissue concentration of contrast medium and the lack of confounding sensitivity to flow artifacts allow CTP to

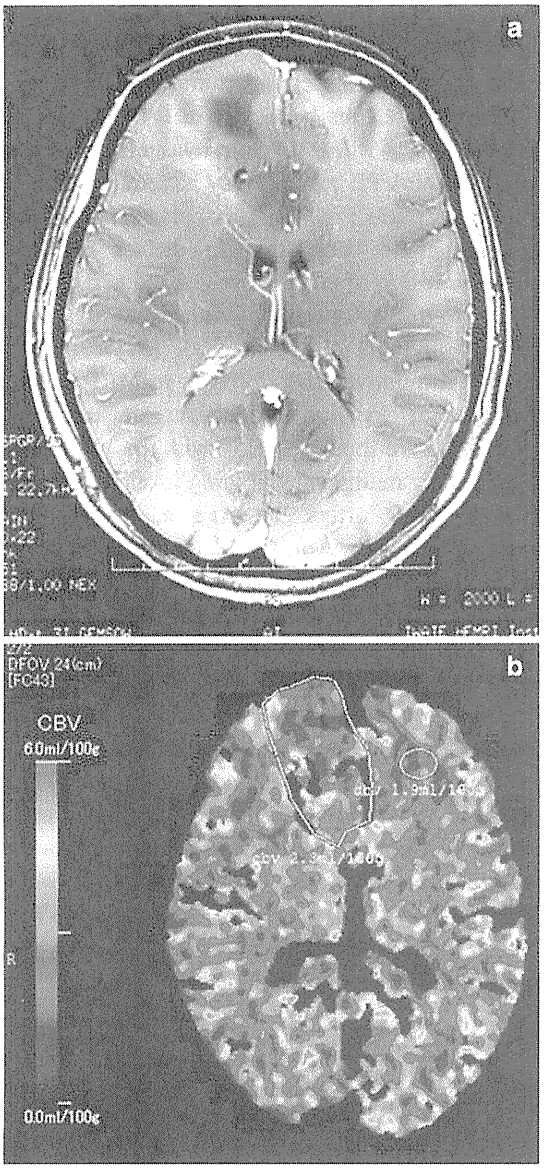

Fig. 4 Gd-T1WI (**a**) and color map of CBV (**b**) for case 14. *Circle* ROI covering the entire tumor bulk and ANWM localized on the nonpathological side

potentially offer a more accurate representation of tissue microvasculature than similar MRP studies [8, 20]. Furthermore, CTP offers advantages such as measurement of quantitative absolute values, greater availability, fast scanning time, high spatial resolution, low cost, and the ability to use this technique for patients who cannot undergo MRI due to the presence of metallic materials in the body [14, 22, 27].

CBF derived from CTP has been suggested to show a tendency toward overestimation, compared with that derived from PET [28]. Since overestimation of CBF in CTP was attributable to the presence of large vessels on the cerebral surface, as contrast materials act as a nondiffusible intravascular tracer in CTP unlike in PET, the VPE method has been proposed to eliminate flow in large vessels [25]. Accurate measurement of CBV contributes to accurate CBF and MTT, as these parameters are closely associated in the central volume principle as CBF = CBV/MTT [29]. We therefore used the VPE method in the present study. We think that optimal threshold differs according to the specific analysis software used for CTP. While VPE threshold was 8.0 ml/100 g in the report by Kudo et al. [25], we established a threshold of 6.0 ml/100 g, since high-CBV areas from cortical large vessels disappeared satisfactorily at this threshold for the analysis software used in our study. Another reason for using the VPE method is that OTs are commonly seen as superficially located tumors in the brain [30, 31]. Elimination of superficial large vessels at the cerebral surface, sulci, and cisterns thus seems warranted when CTP is performed for OTs.

In previous reports of CTP, *r*CBV values ranged from 2.3 to 8.87 ml/100 g for HGG and from 0.95 to 3.28 ml/100 g for LGG, differing significantly between HGG and LGG [13, 14, 20]. The present mean rCBV values in G3 and G2 (Table 2) agreed with previous findings. In addition, mean rCBV values in both G3 and G2 were less than half of 6.0 ml/100 g as VPE threshold. These findings suggest that the VPE method used in this study did not exclude tumor vessels along with other large vessels from CBV maps. While *r*CBV for G3 tended to be on the low side compared with previous reports, this could have resulted from the exclusion of patients with enhancing glioma as subjects in this study. Extravasation of contrast medium through the BBB in enhanced glioma may directly lead to increased CBV, due to the linear relationship between attenuation changes on CT and tissue concentration of contrast medium. Jain et al. [20] documented that *r*CBF and *r*CBV in nonenhancing G3 glioma do not differ significantly from those in nonenhancing G2 glioma, although sample size in that report was small. The present study with more subjects suggested that even nonenhancing G3 glioma retains more vascular density than G2, although the difference in *r*CBV between the two groups was minor (Table 2). However, this result might have been influenced by the disproportionate number of OTs in the G2 (42%) and G3 (83%) groups. If vascular density is significantly higher in G3 OT than in anaplastic astrocytoma, the large number of G3 OTs may have result in a high mean CBV for the G3 group in this study. This issue represents a definite limitation to the present study.

Concentration of contrast medium within the tumor might be subtly influenced by individual parameters such as body size and cardiac output volume, and differences in analytical software among institutes. We must emphasize the importance of estimation using normalized ratios, as

this allows us to ignore these differences. Ellika et al. [22] reported findings for *n*CBV using CTP in 19 patients with glioma, composed of a mixture of enhancing and nonenhancing WHO G1–G4 gliomas, and the utility of *n*CBF and *n*CBV for distinguishing HGG from LGG. They also documented *n*CBF and *n*CBV ranges of 0.78–3.75 and 1.5–3.7 in two patients with nonenhancing G3 glioma, and ranges of 1.26–1.48 and 0.94–1.72 in three patients with nonenhancing G2 glioma, respectively. Mean values of *n*CBF and *n*CBV in G3 and G2 in this study (Table 3) seemed close to the values reported by Ellika et al.

Radiographic grading of gliomas with conventional MRI is not always accurate, with 85.7% sensitivity for predicting HGG, even when including subjects with enhancing glioma [22]. When subjects are limited to those with nonenhancing gliomas, radiographic grading using conventional MRI should be more difficult. A previous report documented 85.7% sensitivity and 100% specificity for identifying HGG using *n*CBV [22]. In the present study, CTP could distinguish nonenhancing G3 glioma from nonenhancing G2 glioma with 83.3% sensitivity and 90.9% specificity using *n*CBV (Fig. 2). This was superior to the results for *n*CBF. Accuracy for distinguishing G3 using *n*CBV in the present study was by no means inferior to that reported by Ellika et al. [22], but subjects in this study were limited to those with nonenhancing glioma. These results suggest that *n*CBV in CTP is useful as an auxiliary examination in addition to routine neuroimaging for predicting the grade of malignancy in nonenhancing gliomas.

Previous studies using MRP have documented higher relative CBV in OT than in other gliomas [32–34]. Lev et al. [33] suggested that OTs tend to appear as high blood volume lesion on MRP, without respect to tumor grade. Two reports using MRP documented that G2 OTs show higher relative CBV than diffuse astrocytoma [32, 34]. Also in a report using CTP by Narang et al. [15], G2 OTs showed a trend towards higher CBV than G2 astrocytic tumors, although no significant difference was found, and no significant difference in CBV between G3 OTs and G2 OTs was identified. Those reports explained the high relative CBV of OT by a hypothesis based on the specific histological features of fine capillary networks [33]. Furthermore, those reports suggested that grading malignancy may be difficult when patients with OT are included, due to a high relative CBV. In the present study, no significant difference in *n*CBV was seen between diffuse astrocytoma and G2 OT, whereas significant differences were found between G3 OT and G2 OT. The difference between the reports described above and the present investigation might be explained by differences between MRP and CTP, and by the use of the VPE method in this study. Signal changes in dynamic susceptibility contrast (DSC) MRI for MRP do not depend on only the concentration of contrast material, but also on T2* or T2 relaxation rates, which are affected by calcified foci and hemorrhage within tumor tissue. These histological features are commonly seen in OTs. DSC signals might thus be higher in OTs than in diffuse astrocytoma, even when the microvascular densities are comparable. The VPE method may have eliminated pixels of high-CBV vessels in OTs, if vascular density in OTs is significantly higher than that in diffuse astrocytoma. However, exclusion of large vessels at the cerebral surface and sulci from CTP maps is important, as OTs grow superficially in the brain. Cha et al. [32] explained for reason of high relative CBV for OTs in MRP by the predominant cortical location in addition to distinct vascular pattern in OTs. We think that CTP with the VPE method is useful for simple malignancy grading in subjects with OTs. Conversely, MRP offers potential advantages for the diagnosis of OTs. However, CTP should not be performed additionally to MRP if the purpose in examination is achieved by MRP, as CTP retains drawbacks such as radiation dose and iodine contrast medium.

The present study possesses some limitations regarding the interpretation of study results. First, the number of patients in this study was small, with remarkably fewer cases of anaplastic astrocytoma compared with OT in G3, as mentioned above. Further investigation including a larger number of cases of anaplastic astrocytoma is needed. A second limitation is the possible discrepancy between histological diagnosis and the region of highest CBV within the tumor. The region targeted for stereotactic biopsy was not rigorously transferred from the region of highest *r*CBV ("hot spots"). However, risk of histological misdiagnosis caused by sampling error during biopsy might be negligible, since the number of patients who underwent biopsy was small in both G3 and G2, and no significant difference in frequency of biopsy was seen between groups. In patients who underwent tumor resection, histological diagnosis was not made using tissue specimens rigorously corresponding to "hot spots." However, histological diagnosis based on the most malignant histological features should be closely associated with high CBV, as increased malignancy is associated with higher vascular density. CTP with a 16-row multidetector CT scanner, covering only four contiguous 8-mm-thick sections, did not cover the entire tumor bulk in some patients. For those patients, histological diagnosis was made using tumor tissues corresponding to the area depicted in CTP. A third limitation was that data calculated from CTP in this study were not the highest CBV values for a small ROI placed in "hot spots" on a color map, but rather were mean values for a large ROI covering the entire tumor bulk. This issue also influences the second limitation. We thought that the simple protocol in this study, combining absolute values as a mean in a large ROI with histological diagnosis from the

area of the most malignant features, is suitable for application in clinical practice, as tissue sampling error of regions corresponding to a small ROI can be avoided. High ICC in inter- and intrarater reliabilities showed that the protocol used in this study offers high reproducibility.

Conclusions

We performed CTP combined with the VPE method for 17 patients, to clarify whether CTP can accurately differentiate between G3 and G2 nonenhancing glioma. Our results showed that *n*CBV from CTP was highly accurate in differentiating G3 from G2 nonenhancing gliomas. The most important result was that CTP enabled differentiation between G3 and G2 nonenhancing OTs. CTP combined with the VPE method offers a useful technique for differentiating between G3 and G2 in nonenhancing gliomas.

Acknowledgments This study was supported in part by a Grant-in-Aid for Advanced Medical Science Research from the Ministry of Science, Education, Sports, and Culture, Japan.

References

1. Louis DN, Ohgaki H, Wiestler OD, Cavenee WK, Burger PC, Jouvet A, Scheithauer BW, Kleihues P (2007) The 2007 WHO classification of tumours of the central nervous system. Acta Neuropathol 114:97–109
2. Dean BL, Drayer BP, Bird CR, Flom RA, Hodak JA, Coons SW, Carey RG (1990) Gliomas: classification with MR imaging. Radiology 174:411–415
3. Ginsberg LE, Fuller GN, Hashmi M, Leeds NE, Schomer DF (1998) The significance of lack of MR contrast enhancement of supratentorial brain tumors in adults: histopathological evaluation of a series. Surg Neurol 49:436–440
4. Mihara F, Numaguchi Y, Rothman M, Kristt D, Fiandaca M, Swallow L (1995) Non-enhancing supratentorial malignant astrocytomas: MR features and possible mechanisms. Radiat Med 13:11–17
5. Jain RK, Gerlowski LE (1986) Extravascular transport in normal and tumor tissues. Crit Rev Oncol Hematol 5:115–170
6. Shweiki D, Itin A, Soffer D, Keshet E (1992) Vascular endothelial growth factor induced by hypoxia may mediate hypoxia-initiated angiogenesis. Nature 359:843–845
7. Vajkoczy P, Menger MD (2000) Vascular microenvironment in gliomas. J Neurooncol 50:99–108
8. Barnett G (2006) High-grade gliomas. Humana, Totowa
9. Law M, Cha S, Knopp EA, Johnson G, Arnett J, Litt AW (2002) High-grade gliomas and solitary metastases: differentiation by using perfusion and proton spectroscopic MR imaging. Radiology 222:715–721
10. Law M, Yang S, Wang H, Babb JS, Johnson G, Cha S, Knopp EA, Zagzag D (2003) Glioma grading: sensitivity, specificity, and predictive values of perfusion MR imaging and proton MR spectroscopic imaging compared with conventional MR imaging. Am J Neuroradiol 24:1989–1998
11. Eastwood JD, Lev MH, Provenzale JM (2003) Perfusion CT with iodinated contrast material. Am J Roentgenol 180:3–12
12. Hoeffner EG, Case I, Jain R, Gujar SK, Shah GV, Deveikis JP, Carlos RC, Thompson BG, Harrigan MR, Mukherji SK (2004) Cerebral perfusion CT: technique and clinical applications. Radiology 231:632–644
13. Ding B, Ling HW, Chen KM, Jiang H, Zhu YB (2006) Comparison of cerebral blood volume and permeability in preoperative grading of intracranial glioma using CT perfusion imaging. Neuroradiology 48:773–781
14. Eastwood JD, Provenzale JM (2003) Cerebral blood flow, blood volume, and vascular permeability of cerebral glioma assessed with dynamic CT perfusion imaging. Neuroradiology 45:373–376
15. Narang J, Jain R, Scarpace L, Saksena S, Schultz LR, Rock JP, Rosenblum M, Patel SC, Mikkelsen T (2010) Tumor vascular leakiness and blood volume estimates in oligodendrogliomas using perfusion CT: an analysis of perfusion parameters helping further characterize genetic subtypes as well as differentiate from astroglial tumors. J Neurooncol. doi:10.1007/s11060-010-0317-3
16. Maia AC Jr, Malheiros SM, da Rocha AJ, Stavale JN, Guimaraes IF, Borges LR, Santos AJ, da Silva CJ, de Melo JG, Lanzoni OP, Gabbai AA, Ferraz FA (2004) Stereotactic biopsy guidance in adults with supratentorial nonenhancing gliomas: role of perfusion-weighted magnetic resonance imaging. J Neurosurg 101:970–976
17. Danchaivijitr N, Waldman AD, Tozer DJ, Benton CE, Brasil Caseiras G, Tofts PS, Rees JH, Jager HR (2008) Low-grade gliomas: do changes in rCBV measurements at longitudinal perfusion-weighted MR imaging predict malignant transformation? Radiology 247:170–178
18. Price SJ (2010) Advances in imaging low-grade gliomas. Adv Tech Stand Neurosurg 35:1–34
19. Nabavi DG, Cenic A, Craen RA, Gelb AW, Bennett JD, Kozak R, Lee TY (1999) CT assessment of cerebral perfusion: experimental validation and initial clinical experience. Radiology 213: 141–149
20. Jain R, Ellika SK, Scarpace L, Schultz LR, Rock JP, Gutierrez J, Patel SC, Ewing J, Mikkelsen T (2008) Quantitative estimation of permeability surface-area product in astroglial brain tumors using perfusion CT and correlation with histopathologic grade. Am J Neuroradiol 29:694–700
21. Jain R, Scarpace L, Ellika S, Schultz LR, Rock JP, Rosenblum ML, Patel SC, Lee TY, Mikkelsen T (2007) First-pass perfusion computed tomography: initial experience in differentiating recurrent brain tumors from radiation effects and radiation necrosis. Neurosurgery 61:778–786
22. Ellika SK, Jain R, Patel SC, Scarpace L, Schultz LR, Rock JP, Mikkelsen T (2007) Role of perfusion CT in glioma grading and comparison with conventional MR imaging features. Am J Neuroradiol 28:1981–1987
23. Sasaki M, Kudo K, Ogasawara K, Fujiwara S (2009) Tracer delay-insensitive algorithm can improve reliability of CT perfusion imaging for cerebrovascular steno-occlusive disease: comparison with quantitative single-photon emission CT. Am J Neuroradiol 30:188–193
24. Wintermark M, Maeder P, Thiran JP, Schnyder P, Meuli R (2001) Quantitative assessment of regional cerebral blood flows by perfusion CT studies at low injection rates: a critical review of the underlying theoretical models. Eur Radiol 11:1220–1230
25. Kudo K, Terae S, Katoh C, Oka M, Shiga T, Tamaki N, Miyasaka K (2003) Quantitative cerebral blood flow measurement with dynamic perfusion CT using the vascular-pixel elimination method: comparison with H2(15)O positron emission tomography. Am J Neuroradiol 24:419–426
26. Shrout PE, Fleiss JL (1979) Intraclass correlations: uses in assessing rater reliability. Psychol Bull 86:420–428
27. Miles KA, Charnsangavej C, Lee FT, Fishman EK, Horton K, Lee TY (2000) Application of CT in the investigation of angiogenesis in oncology. Acad Radiol 7:840–850